IEICE TRANS. ELECTRON., VOL.E101–C, NO.7 JULY 2018

INVITED PAPER *Special Section on Distinguished Papers in Photonics*

Multimodal Interference in Perfluorinated Polymer Optical Fibers: Application to Ultrasensitive Strain and Temperature Sensing*

Yosuke MIZUNO[†a)], ***Member***, **Goki NUMATA**[†], **Tomohito KAWA**[†], **Heeyoung LEE**[†], **Neisei HAYASHI**[††], ***Nonmembers***, ***and*** **Kentaro NAKAMURA**[†], ***Member***

SUMMARY We review the recent advances on strain and temperature sensing techniques based on multimodal interference in perfluorinated (PF) graded-index (GI) polymer optical fibers (POFs). First, we investigate their fundamental characteristics at 1300 nm. When the core diameter is 62.5 μm, we obtain strain and temperature sensitivities of −112 pm/$\mu\varepsilon$ and +49.8 nm/°C, the absolute values of which are, by simple calculation, approximately 13 and over 1800 times as large as those in silica GI multimode fibers, respectively. These ultra-high strain and temperature sensitivities probably originate from the unique PF polymer used as core material. Subsequently, we show that the temperature sensitivity (absolute value) is significantly enhanced with increasing temperature toward ∼70°C, which is close to the glass-transition temperature of the core polymer. When the core diameter is 62.5 μm, the sensitivity at 72°C at 1300 nm is 202 nm/°C, which is approximately 26 times the value obtained at room temperature and >7000 times the highest value previously reported using a silica multimode fiber. Then, we develop a single-end-access configuration of this strain and temperature sensing system, which enhances the degree of freedom in embedding the sensors into structures. The light Fresnel-reflected at the distal open end of the POF is exploited. The obtained strain and temperature sensitivities are shown to be comparable to those in two-end-access configurations. Finally, we discuss the future prospects and give concluding remarks.

key words: *polymer optical fibers, perfluorinated polymer, modal interference, strain sensing, temperature sensing*

1. Introduction

Strain and temperature sensing using optical fibers has been an active research area because of light weight, small size, and insensitivity to ambient electromagnetic fields. While a number of methods exploiting fiber Bragg gratings (FBGs) [1], [2], long-period gratings (LPGs) [3], [4], Raman scattering [5], [6], and Brillouin scattering [7]–[11] have been developed, one of the simple and low-cost implementations is based on the interference among guided modes of a multimode fiber (MMF). Since Mehta et al [12] reported the first demonstration in 2003, to date, various structures have been proposed, as well summarized in Table 1 in Ref. [13]. Among them, the most typical is a so-called single-mode-multimode-single-mode (SMS) structure [14]–[16], where an MMF is sandwiched between two single-mode fibers (SMFs).

Manuscript received September 27, 2017.
Manuscript revised December 22, 2017.
*This is a review article.
†The authors are with Institute of Innovative Research, Tokyo Institute of Technology, Yokohama-shi, 226–8503 Japan.
††The author is with Research Center for Advanced Science and Technology, The University of Tokyo, Tokyo, 153–8904 Japan.
a) E-mail: ymizuno@sonic.pi.titech.ac.jp
DOI: 10.1587/transele.E101.C.602

Based on the SMS structure comprising a 1.8-m-long silica graded-index (GI-) MMF, Liu et al [14] have obtained a strain sensitivity of +18.6 pm/$\mu\varepsilon$ and a temperature sensitivity of +58.5 pm/°C at 1550 nm. Tripathi et al [15] have shown that not only the absolute values but also the signs of the strain and temperature sensitivities are highly dependent on the structure (e.g., core diameter) and the material (e.g., dopant) of silica MMFs. Recently, in order to enhance the maximal measurable strain, Huang et al [17] have developed a large-strain sensor using a 0.16-m-long polymethyl methacrylate (PMMA)-based step-index plastic optical fiber (POF) as an MMF, and obtained strain and temperature sensitivities of −1.72 pm/$\mu\varepsilon$ and +56.8 pm/°C, respectively, at 1570 nm. However, the propagation loss of PMMA-based POFs at telecommunication wavelength is so high ($\gg 1 \times 100$ dB/m) that the maximal sensing range is inherently limited to several tens of meters. Besides, discriminative measurement of strain and temperature is also important for practical use; it can be theoretically achieved by combined use of multimode interference and another physical phenomenon, such as Brillouin scattering, which has, however, not been observed in PMMA-based POFs. Perfluorinated graded-index (PFGI-) POFs [18] are the only POFs that have a relatively low loss of ∼0.25 dB/m at 1550 nm (or ∼0.05 dB/m at 1300 nm) in which Brillouin scattering has been experimentally observed [19]–[23].

In this work, first, we implement the strain and temperature sensors based on the SMS structure comprising a PFGI-POF and investigate their sensing performance at 1300 nm [24]. Three 1-m-long PFGI-POFs with core diameters of 50, 62.5, and 120 μm are used. When the core diameter is 62.5 μm, the strain sensitivity is −112 pm/$\mu\varepsilon$, the absolute value of which is, by simple calculation, approximately 13 times as large as that in a silica GI-MMF (this calculation is based on the assumption that the sensitivity is linearly dependent on optical wavelength and MMF length, which has now been clarified to be incorrect [15], [25]; however, as no fair method of comparison has not been established yet, we will use this simple evaluation in this paper). The temperature sensitivity at room temperature is +49.8 nm/°C, which is over 1800 times as large as that in a silica GI-MMF. Next, we investigate the performance of temperature sensors composed of 1-m-long PFGI-POFs in a wide temperature range from room temperature to high temperature around the glass-transition temperature [26]. When the core diameter is 62.5 μm, the temperature sensitivity (ab-

solute value) increases with increasing temperature, reaching +202 nm/°C at ~72°C, which is 26 times as high as that at room temperature. This behavior is confirmed to be unique to POFs with relatively low glass-transition temperature. Then, by using Fresnel reflection at the distal open end of the PFGI-POF, we develop a single-end-access configuration of this strain and temperature sensors [25]. We experimentally show that when the length of the PFGI-POF is the same, the strain and temperature sensitivities do not largely change regardless of the configurations (i.e., either single- or two-end access). This single-end-access configuration will enhance the degree of freedom in embedding the sensors into structures. Finally, we discuss future prospects and present concluding remarks.

2. Principle

The SMS structure consists of an MMF connected at both ends to identical SMFs. At the first SMF/MMF boundary, light is injected into the MMF through the lead-in SMF. As the spot size of the fundamental mode of the MMF is generally different from that of the SMF, the first few modes of the MMF are excited and propagate through the MMF with their respective propagation constants. At the second SMF/MMF boundary, the net field coupled from these modes to the lead-out SMF is determined by the relative phase differences among various modes of the MMF. When the fibers are axially aligned at the first SMF/MMF boundary, only the axially symmetric modes of the MMF are excited. According to the detailed calculation [16], the optical power in the lead-out SMF can be expressed as

$$P_{\text{out}} = |a_0^2 + a_1^2 \exp i(\beta_0 - \beta_1)L + a_2^2 \exp i(\beta_0 - \beta_2)L + \cdots|^2, \quad (1)$$

where a_i is the field amplitude of the i-th mode at the first SMF/MMF boundary, β_i is the propagation constant of the i-th mode, and L is the length of the MMF. Equation (1) indicates that the optical power in the lead-out SMF is affected by physical changes (such as strain and temperature) influencing the propagation constants and the length of the MMF. By measuring this shift either in terms of power or the spectral location of peak/dip, the changes can be quantitatively obtained.

3. Fundamental Characterization

3.1 Experimental Setup

Three 1-m-long PFGI-POFs with different core diameters of 50, 62.5, and 120 μm were employed. The core and cladding layers are composed of doped and undoped polyperfluorobutenylvinyl ether, respectively. The refractive index at the center of the core is 1.356, whereas that of the cladding layer is 1.342 [27]. The polycarbonate reinforcement overcladding layer (diameter: 500 μm) reduces microbending losses and increases the load-bearing capability.

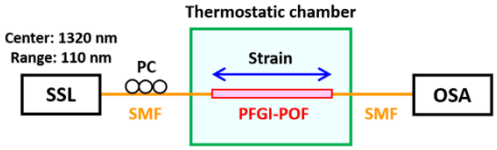

Fig. 1 Schematic of experimental setup. OSA, optical spectrum analyser; PC, polarization controller; PFGI-POF, perfluorinated graded-index plastic optical fiber; SMF, single-mode fiber; SSL, swept-source laser. Reproduced with permission from Ref. [24]; copyright (2014) IEEE.

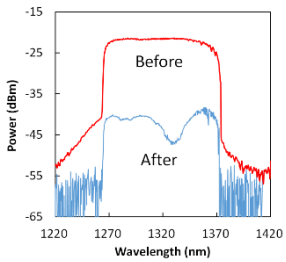

Fig. 2 Measured optical spectra before and after transmission through the POF. Reproduced with permission from Ref. [24]; copyright (2014) IEEE.

The numerical aperture is 0.185, and the propagation loss is ~0.25 dB/m at 1550 nm and ~0.05 dB/m at 1300 nm.

Figure 1 depicts the experimental setup. The PFGI-POF was connected to silica SMFs by butt-coupling [19]. A swept-source laser (SSL) was used as a light source, which can be regarded as a broadband source with a central wavelength of 1320 nm and a bandwidth of 110 nm. The laser output was, after polarization adjustment, launched into the PFGI-POF, and the transmitted light spectrum was monitored with an optical spectrum analyzer (OSA). Strain and temperature change were applied to the whole length of the PFGI-POF. The room temperature was ~27°C.

3.2 Experimental Results

Figure 2 shows the measured optical spectra before and after transmission through the PFGI-POF with 62.5-μm core diameter. A characteristic dip was clearly observed at around 1330 nm in the latter spectrum.

The measured dependence of this spectral dip on strain is shown in Fig. 3 (a). With increasing applied strain, the spectral dip shifted to shorter wavelength. Figure 3 (b) shows the dip wavelength plotted as a function of strain. The dependence was almost linear with a coefficient of −1118 nm/% (= −112 pm/$\mu\varepsilon$), the absolute value of which is approximately 13 and 7.7 times as large as those in a silica GI-MMF [14] and a PMMA-based POF [17], respectively. In the same way, as temperature increased, this spectral dip shifted to longer wavelength, as shown in Fig. 3 (c). Figure 3 (d) shows the dip wavelength dependence on temperature, leading to a coefficient of +49.8 nm/°C, which is over 1800 and 100 times as large as those in a silica GI-MMF [14] and a PMMA-based POF [17], respectively.

We also performed the same measurement using

the PFGI-POFs with 50-μm and 120-μm core diameters, and obtained the strain and temperature coefficients of +3.42 pm/$\mu\varepsilon$ and −4.71 nm/°C (50-μm core), and −8.21 pm/$\mu\varepsilon$ and +0.74 nm/°C (120-μm core), respectively. These values were much larger than those in silica GI-MMFs with the same core diameters, but not as large as that in the PFGI-POF with 62.5-μm core diameter. This is partially because the critical wavelength [15] with 62.5-μm core diameter is located closer to ∼1300 nm (measured wavelength region) than those with 50-μm and 120-μm core diameters.

Considering that SMS-based sensors using silica GI-MMFs with the same core diameters do not have large strain and temperature coefficients, these ultra-high strain and temperature sensitivities of the PFGI-POF (especially with 62.5-μm core) probably originate not from its structure but from its unique material (PF polymer). In other words, the propagation constant of each mode and the length in perfluorinated polymer are much more highly dependent on strain and temperature than those in other MMFs (either glass or polymer).

Thus, in this Section, the strain and temperature sensors based on modal interference in the SMS structure comprising a PFGI-POF was implemented, and their basic sensing performance was investigated using an SSL at around 1300 nm. When the core diameter was 62.5 μm, the strain and temperature sensitivities were −112 pm/$\mu\varepsilon$ and +49.8 nm/°C, the absolute values of which were approximately 13 and > 1800 times as large as those in a silica GI-MMF. We believe that the ultra-high temperature sensitivity of this sensor is attractive for such fields as will require precise temperature measurement. We also point out that the difference in sign between the strain and temperature coefficients will potentially lead to extremely accurate Brillouin-combined discriminative (not distributed) measurement of strain and temperature [28].

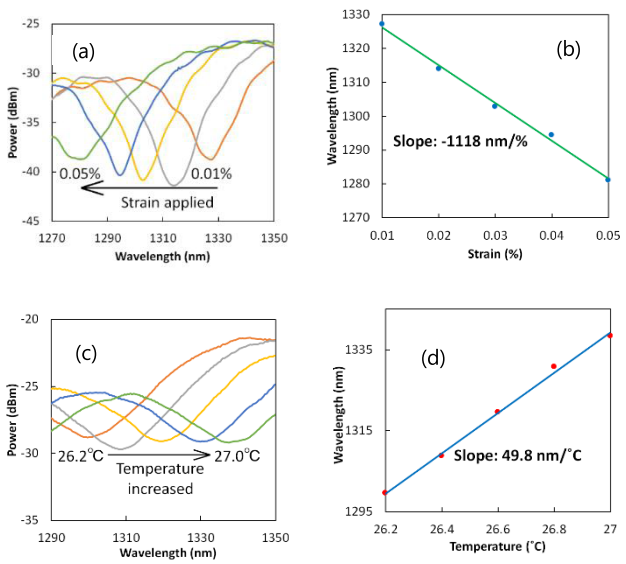

Fig. 3 Measurement results for the POF with 62.5-μm core: (a) spectral dependence on strain, (b) dip wavelength vs strain, (c) spectral dependence on temperature, and (d) dip wavelength vs temperature. Reproduced with permission from Ref. [24]; copyright (2014) IEEE.

4. Temperature Sensitivity Enhancement

4.1 Experimental Setup

The same 1-m-long PFGI-POFs with three different core diameters (50, 62.5, and 120 μm) were used as the MMFs. The experimental setup for characterizing the PFGI-POF-based temperature sensors in a wide temperature range was basically the same as that shown in Fig. 1. Both ends of the PFGI-POF were butt-coupled to silica SMFs [19], and the whole length of the PFGI-POF was placed in a thermostatic chamber to control the ambient temperature. One important difference from Fig. 1 is the light source. As spectral measurement with as wide a span as possible is preferable in this experiment, we employed an ultra-wideband source (UWS-1000, Santec) that emits super-continuum light with an output spectrum from 1100 to 1760 nm (pumped at 1550 nm). Its spectral power density was higher than −30 dBm/nm over the full range; this value is much larger than that of a standard white-light source, which cannot be used because of the high propagation loss of the PFGI-POF. The UWS output was injected into the PFGI-POF, and the transmission spectrum was measured using an OSA. The room temperature was 20°C.

4.2 Experimental Results

The measured optical spectra before and after transmission of the PFGI-POF with 50-μm core diameter at room temperature are shown in Fig. 4. Before transmission, a relatively flat spectrum ranging from 1100 to 1760 nm was observed. The peak at 1550 nm corresponds to the pump frequency of the super-continuum generation. After transmission, not only ∼10–20-dB relatively uniform loss but also wavelength-dependent loss was observed in the spectrum, resulting in the several characteristic dips and peaks. These dips and peaks originate from the modal interference, and their wavelengths are dependent on the ambient temperature of the POF.

We then investigated the wide-range temperature de-

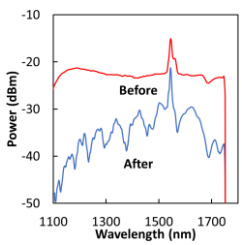

Fig. 4 Measured optical spectra before and after transmission through the PFGI-POF. Copyright (2015) The Japan Society of Applied Physics (JSAP).

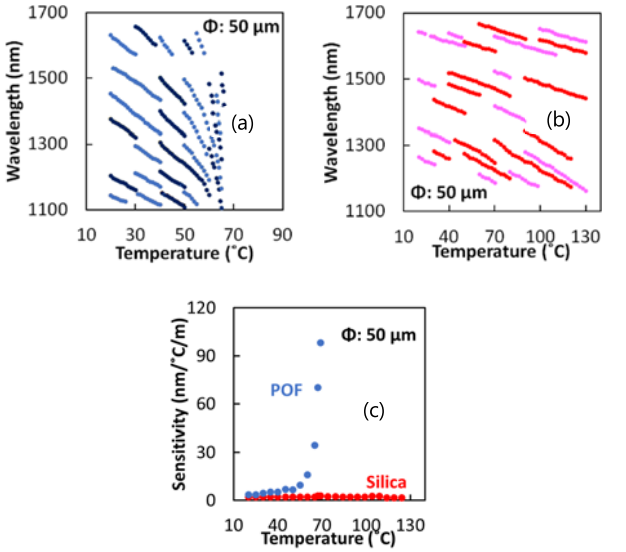

Fig. 5 Dip-wavelength dependence on wide-range temperature in (a) the PFGI-POF and (b) the silica GI-MMF with 50-μm core diameter. Different colors were used to clarify different dips. (c) Temperature sensitivity (absolute value of the temperature-dependence coefficients) at 1300 nm in the PFGI-POF and the silica GI-MMF plotted as functions of temperature. Copyright (2015) JSAP.

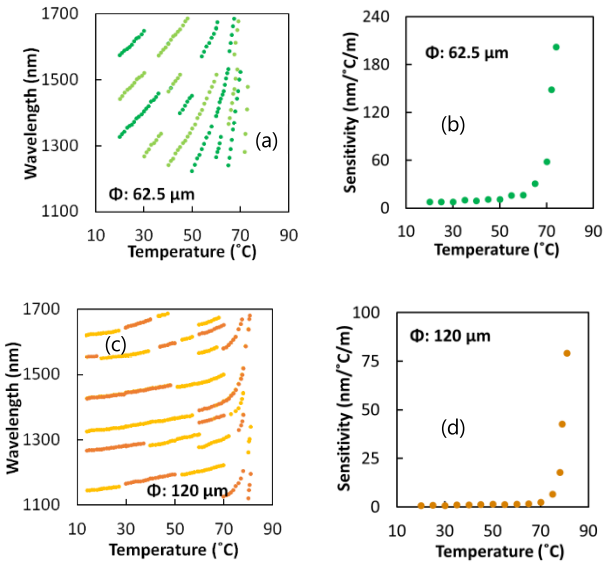

Fig. 6 Temperature dependences of (a) the dip wavelengths and (b) the coefficient in the PFGI-POF with 62.5-μm core diameter, and (c,d) those in the PFGI-POFs with 120-μm core diameter. Copyright (2015) JSAP.

pendence of the wavelengths of some relatively clear spectral dips in the PFGI-POF with 50-μm core diameter (Fig. 5 (a)). The measured data are discontinuously plotted because of the two reasons: (1) measurement at one fixed temperature took ~10 min since we needed to wait for the temperature to be stable. Therefore, the measurements were performed in every 10°C range separately (i.e., 20–30°C, 30–40°C, ...), with their data merged later (some peaks appeared or disappeared with time on account of the polarization fluctuations [14]; this instability could be mitigated by employing polarization diversity or polarization scrambling); (2) when the dips shifted close to the 1550-nm pump peak, they were buried by the spectral floor (this problem could be resolved by use of a properly designed optical filter at 1550 nm). As shown in Fig. 5 (a), with increasing temperature, all the dip wavelengths decreased. The dependence coefficient at room temperature at 1300 nm was approximately −5.3 nm/°C (calculated by interpolation/extrapolation), which moderately agrees with the previously reported value (−4.7 nm/°C) [24]. The absolute values of the coefficients at shorter wavelengths were slightly smaller than those at longer wavelengths in this wavelength range, which indicates that the critical wavelength [15] is longer than ~1700 nm. In the temperature range from 20 to ~50°C, the dependence coefficient of any of the dips was kept almost constant, but over ~50°C, their absolute values gradually became larger. The coefficient at 67°C at 1300 nm reached −85 nm/°C, which was ~16 times the value at room temperature. Over ~67°C, the spectral change was so drastic that correct measurement was no longer performed.

Subsequently, we confirmed that this peculiar behavior is a unique characteristic to POFs by performing the same measurement using a silica GI-MMF with the same core diameter (50 μm). Figure 5 (b) shows the dip wavelengths measured as functions of temperature ranging from 20 to 130°C. The dependence coefficient at room temperature at 1300 nm (−2.2 nm/°C) was close to that at ~130°C (−2.3 nm/°C), which indicates that the temperature-dependent gradual change in the coefficients (in this temperature range) is unique to POFs. This behavior, similar to the nonlinear temperature dependence of the Brillouin frequency shift in POFs [29], seems to have been caused by the partial phase transition of the polymer material. The temperature of ~67°C, at which the largest coefficient (absolute value) was obtained in the PFGI-POF, probably corresponds to the glass transition temperature of the polyperfluorobutenylvinyl ether (~108°C; note that the phase transition, which has some influence on the thermal expansion coefficient and each modal index, generally occurs in the temperature range of roughly 50°C in polymers [27] and that the starting temperature of phase transition is lower than the glass transition temperature by several tens of degrees). Figure 5 (c) shows the temperature sensitivities, i.e., the absolute values of the temperature-dependence coefficients of the dip wavelength, at 1300 nm in the PFGI-POF and the silica GI-MMF plotted as functions of temperature. It is clear that the temperature sensitivity in the PFGI-POF abruptly grows large at 67°C, while that in the silica GI-MMF remains almost constant.

We also performed the same measurements using the PFGI-POFs with 62.5-μm and 120-μm core diameters (Fig. 6 (a)–(d)). In both cases, with an increase in temperature, the dip wavelengths increased. The difference not only in the absolute value but also in the sign has been already reported [24] and explained by the structural influence on the critical wavelengths [15] (which are shorter than 1100 nm

for the 62.5-μm-core PFGI-POF and longer than 1700 nm for the 120-μm-core PFGI-POF). The coefficients at room temperature at 1300 nm were +7.7 nm/°C for the 62.5-μm-core PFGI-POF and +1.1 nm/°C for the 120-μm-core PFGI-POF. The difference between these values and those previously reported [24] is probably caused by the manually prepared end-surfaces and lot-to-lot non-uniformity, leading to the different excited modes. The maximal values obtained at high temperature at 1300 nm were +202 nm/°C for the 62.5-μm-core PFGI-POF and +85.6 nm/°C for the 120-μm-core PFGI-POF, which are ~26 and ~78 times larger than those at room temperature, respectively. The temperature sensitivity at 1300 nm of +202 nm/°C, obtained at ~72°C using the 62.5-μm-core PFGI-POF, is well over 7000 times the largest value previously reported using a silica GI-MMF [14] and is, to the best of our knowledge, the highest value ever reported in modal-interference-based temperature sensors. Note that, although the dependence is nonlinear, the wavelength of a certain dip is in one-to-one correspondence with temperature, which can be exploited for temperature sensing (we need to be careful in designing the system because the measurement error is expected to vary with temperature). The temperatures at which the largest temperature sensitivities (absolute values of the temperature-dependence coefficients) were experimentally obtained were ~69, ~72, and ~82°C in the PFGI-POFs with 50-, 62.5-, and 120-μm core diameters, respectively, suggesting a positive correlation between the highest operable temperature and the core diameter of the POF.

Thus, in this Section, we investigated the performance of SMS-based temperature sensors comprising 1-m-long PFGI-POFs with 50-, 62.5-, and 120-μm core diameters in a wide temperature range. When the core diameter is 62.5 μm, with an increase in temperature, the temperature sensitivity, i.e., the temperature-dependence coefficients of the spectral dips, increased, reaching +202 nm/°C at ~72°C at 1300 nm, which was over 26 times the value obtained at room temperature. Over ~72°C, correct measurement was difficult due to the spectral instability. We verified that this behavior is unique to POFs with relatively low glass-transition temperature by demonstrating that the temperature sensitivity of a silica-MMF-based sensor shows almost no change with increasing temperature up to 130°C. Besides, considering that the phase-transition temperature of polymers can be controlled by adding plasticizers and by copolymerizing/blending different materials [30], we expect that such an ultra-high temperature sensitivity will be achievable not only around 70–80°C but also around somewhat arbitrary temperature, opening up the way for more useful and practical applications.

5. Single-End-Access Configuration

5.1 Motivation

Substantial efforts have been made to improve the performance of SMS-based strain and temperature sensors, but almost all the SMS-based sensors reported thus far are two-end-access systems, in which both ends of the MMF are physically connected to SMFs (Fig. 7 (a)). From a practical viewpoint, single-end-access configurations (Fig. 7 (b)) with an enhanced degree of freedom in embedding the sensors into structures are preferable. There are only three examples of such single-end-access configurations; the first is a displacement sensor reported by Mehta et al [12], which comprises an SMF-MMF-airgap-mirror structure. It is, however, difficult to directly employ this structure to measure strain and temperature; in addition, use of the mirror reduces the ease of handling. The second is a temperature sensor reported by Li et al [31], in which no descriptions on strain sensing capability have been provided at all. The third is a strain sensor reported by Ribeiro et al [32], in which strain is measured based on modulated power; its operating principle is quite different from that of other frequency-based SMS sensors.

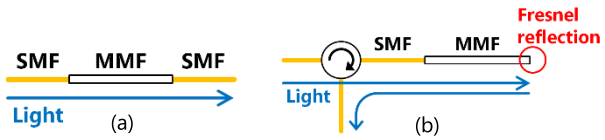

Fig. 7 Conceptual setups of (a) transmissive configuration and (b) reflectometric configuration. MMF, multimode fiber; SMF, single-mode fiber.

Fig. 8 Actual experimental setups of (a) transmissive configuration and (b) reflectometric configuration. OSA, optical spectrum analyzer; PFGI-POF, perfluorinated graded-index polymer optical fiber; PSCR, polarization scrambler; SSL, swept-source laser. The yellow lines indicate silica single-mode fibers.

Here, by using Fresnel reflection at the distal open end of the MMF, we develop a single-end-access configuration of SMS-based strain and temperature sensing systems, in which PFGI-POFs were employed as MMFs to obtain high sensitivities. We experimentally show that when the MMF length is the same, the strain and temperature sensitivities do not largely change regardless of the configurations (i.e., either single- or two-end access).

5.2 Experimental Setup

The same type of PFGI-POF with a core diameter of 62.5 μm was used as the MMF. The POF length is 0.7 m. The actual experimental setups of transmissive (for comparison) and reflectometric configurations are shown in Fig. 8 (a) and 8 (b), respectively. In both configurations, an SSL with a 20-kHz sweep rate was employed as a broadband light source with a central wavelength of 1320 nm and a bandwidth of 110 nm. The laser output was first input to a polarization controller to suppress the polarization-dependent spectral fluctuations, and then injected into the

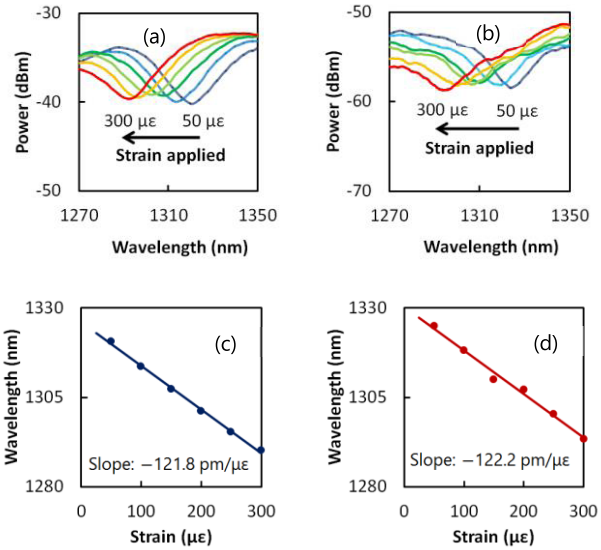

Fig. 9 Measured spectral dependences on strain in (a) transmissive configuration and (b) reflectometric configuration. The dip wavelength dependences on strain in (c) transmissive configuration and (d) reflectometric configuration.

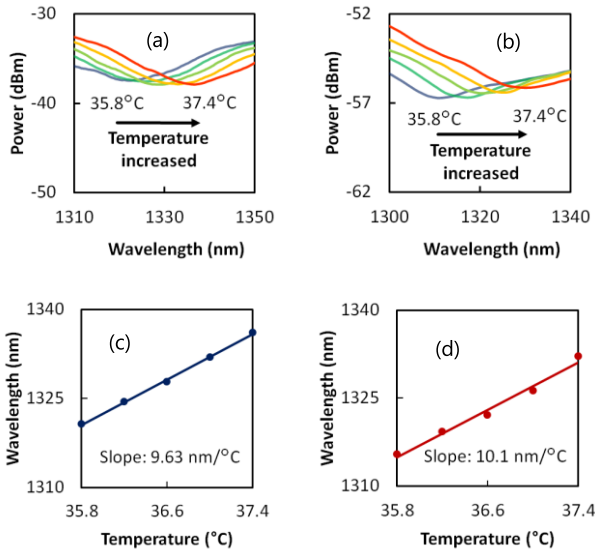

Fig. 10 Measured spectral dependences on temperature in (a) transmissive configuration and (b) reflectometric configuration. The dip wavelength dependences on temperature in (c) transmissive configuration and (d) reflectometric configuration.

POF. In Fig. 8 (a), both ends of the POF were butt-coupled to silica SMFs [19], and the spectrum of the transmitted light was monitored using an OSA. In contrast, in Fig. 8 (b), one end of the POF was butt-coupled to a silica SMF in the same way, but the other end was kept open (flatly polished); the spectrum of the reflected light was monitored using an OSA. Note that the optical circulator used in Fig. 8 (b) had an operating wavelength of 1280 to 1340 nm and insertion losses of approximately 0.5 dB for both directions (i.e., port 1 to port 2 and port 2 to port 3). In both cases, the entire length of the POF was strained or heated. The room temperature was approximately 28°C.

5.3 Experimental Results

The measured dependences of the spectral dips on strain in transmissive and reflectometric configurations are shown in Fig. 9 (a) and 9 (b), respectively. In both cases, a relatively broad single dip was observed in this range, which shifted to shorter wavelengths with increasing applied strain. The spectral power in Fig. 9 (b) was approximately 20 dB lower than that in Fig. 9 (a); this is valid considering the loss of Fresnel reflection at the POF end (~2.2% reflection, corresponding to a 16.5 dB loss; by a simple calculation based only on the core refractive index difference) and the additional POF propagation loss (if compared with the Fresnel loss, negligibly low with this short POF (0.7 m)). In the reflectometric configuration, if necessary, we could form a mirror at the open end of the POF to increase the spectral power. Figures 9 (c) and 9 (d) show the dip wavelengths plotted as functions of strain. The dependences were both almost linear with slopes of −1218 nm/% (= −121.8 pm/$\mu\varepsilon$; transmissive) and −1222 nm/% (= −122.2 pm/$\mu\varepsilon$; reflectometric). These values moderately agree with the previously reported value [24]; the discrepancy probably originates from the imperfect end faces, asymmetric coupling to the SMFs, and longitudinal structural non-uniformity of the POF.

Subsequently, the dependences of the dip on temperature were also measured (Figs. 10 (a) (transmissive) and 10 (b) (reflectometric)). The dips shifted to shorter wavelengths as temperature increased. The dip wavelengths plotted as functions of temperature (Figs. 10 (c) and 10 (d)) indicate that the temperature-dependence coefficients were 9.63 nm/°C (transmissive) and 10.1 nm/°C (reflectometric); these values are also consistent with those previously reported [24]. Thus, the reflectometric configuration was experimentally proved to possess almost the same strain and temperature sensitivities as those of transmissive configuration with an advantage of single-end accessibility. One concern is that when the POF length is longer than several dozen meters, the additional propagation loss may result in the reflected spectrum buried by the noise floor. This problem could be mitigated by attaching a mirror at the end of the POF.

Thus, in this Section, a single-end-access configuration of SMS-based strain and temperature sensing systems exploiting Fresnel reflection at the distal open end of the MMF (PFGI-POF) was developed. High strain and temperature sensitivities of −122.2 pm/$\mu\varepsilon$ and 10.1 nm/°C, respectively, were obtained. These values were comparable to those in the two-end-access configuration. This result implied that, in analyzing the performance of SMS-based sensors, we should take into consideration not only the (relatively fundamental) two modes but also many other modes simultaneously (see Appendix of Ref. [25]). We anticipate that our method will drastically enhance the ease of handling of SMS-based fiber-optic sensors.

6. Conclusion

Recent advances on the strain and temperature sensing based on the SMS structure comprising a PFGI-POF were presented. First, the fundamental sensing characteristics were investigated at 1300 nm. Three 1-m-long PFGI-POFs with core diameters of 50, 62.5, and 120 μm were tested. When the core diameter was 62.5 μm, the strain sensitivity was $-112\,\mathrm{pm}/\mu\varepsilon$, the absolute value of which was approximately 13 times as large as that in a silica GI-MMF. The temperature sensitivity at room temperature was +49.8 nm/°C, which was over 1800 times as large as that in a silica GI-MMF. Subsequently, the performance of temperature sensors composed of 1-m-long PFGI-POFs in a wide temperature range from room temperature to high temperature (around the glass-transition temperature) was investigated. When the core diameter was 62.5 μm, the temperature sensitivity (absolute value) increased with increasing temperature, reaching +202 nm/°C at ∼72°C, which was 26 times as high as that at room temperature. By showing that the temperature sensitivity of a silica MMF-based sensor does not change with increasing temperature to 130°C, this behavior was verified to be unique to POFs with relatively low glass-transition temperature. Finally, by using Fresnel reflection at the distal open end of the PFGI-POF, a single-end-access configuration of this strain and temperature sensors was implemented. We experimentally proved that when the length of the PFGI-POF is the same, the strain and temperature sensitivities do not largely change regardless of the configurations (i.e., either single- or two-end access).

In addition to these achievements, we have found that the strain and temperature sensitivities do not largely depend on the length of the MMF [25], that the temperature sensitivity at room temperature can be enhanced by annealing [33] and that the modal interference in partially chlorinated GI POFs is potentially applicable to high-sensitivity temperature measurement with low strain sensitivity [34]. Future tasks include clarification of the critical wavelength dependence on fiber properties [15] (which will be a useful guideline for the researchers who search for new materials with high sensitivities), extremely large strain sensing with plastic deformation [35], clarification of the shortest length of the MMF, clarification of cross effect of strain and temperature [36], and discriminative (not distributed) sensing of strain, temperature, and some other parameters by combined use of FBG and/or Brillouin scattering. We anticipate that this review paper will be a good basis for researchers working on POF-based SMS sensing technology.

References

[1] A.D. Kersey, M.A. Davis, H.J. Patrick, M. LeBlanc, K.P. Koo, C.G. Askins, M.A. Putnam, and E.J. Friebele, "Fiber grating sensors," J. Lightwave Technol., vol.15, no.8, pp.1442–1463, 1997.

[2] B.-O. Guan, H.-Y. Tam, X.-M. Tao, and X.-Y. Dong, "Simultaneous strain and temperature measurement using a superstructure fiber Bragg grating," IEEE Photon. Technol. Lett., vol.12, no.6, pp.675–677, 2000.

[3] V. Bhatia and A.M. Vengsarkar, "Optical fiber long-period grating sensors," Opt. Lett., vol.21, no.9, pp.692–694, 1996.

[4] Y.-P. Wang, L. Xiao, D.N. Wang, and W. Jin, "Highly sensitive long-period fiber-grating strain sensor with low temperature sensitivity," Opt. Lett., vol.31, no.23, pp.3414–3416, 2006.

[5] M.A. Farahani and T. Gogolla, "Spontaneous Raman scattering in optical fibers with modulated probe light for distributed temperature Raman remote sensing," J. Lightwave Technol., vol.17, no.8, pp.1379–1391, 1999.

[6] M.N. Alahbani, Y.T. Cho, and T.P. Newson, "Simultaneous temperature and strain measurement with combined spontaneous Raman and Brillouin scattering," Opt. Lett., vol.30, no.11, pp.1276–1278, 2005.

[7] T. Horiguchi and M. Tateda, "BOTDA-nondestructive measurement of single-mode optical fiber attenuation characteristics using Brillouin interaction: theory," J. Lightwave Technol., vol.7, no.8, pp.1170–1176, 1989.

[8] T. Kurashima, T. Horiguchi, H. Izumita, S. Furukawa, and Y. Koyamada, "Brillouin optical-Fiber time domain reflectometry," IEICE Trans. Commun., vol.E76-B, pp.382–390, 1993.

[9] D. Garus, K. Krebber, F. Schliep, and T. Gogolla, "Distributed sensing technique based on Brillouin optical-fiber frequency-domain analysis," Opt. Lett., vol.21, no.17, pp.1402–1404, 1996.

[10] K. Hotate and T. Hasegawa, "Measurement of Brillouin gain spectrum distribution along an optical fiber using a correlation-based technique - proposal, experiment and simulation," IEICE Trans. Electron., vol.E83-C, pp.405–412, 2000.

[11] Y. Mizuno, W. Zou, Z. He, and K. Hotate, "Proposal of Brillouin optical correlation-domain reflectometry (BOCDR)," Opt. Express, vol.16, no.16, pp.12148–12153, 2008.

[12] A. Mehta, W. Mohammed, and E.G. Johnson, "Multimode interference-based fiber-optic displacement sensor," IEEE Photon. Technol. Lett., vol.15, no.8, pp.1129–1131, 2003.

[13] O. Frazão, S.O. Silva, J. Viegas, L.A. Ferreira, F.M. Araújo, and J.L. Santos, "Optical fiber refractometry based on multimode interference," Appl. Opt., vol.50, no.25, pp.E184–E188, 2011.

[14] Y. Liu and L. Wei, "Low-cost high-sensitivity strain and temperature sensing using graded-index multimode fibers," Appl. Opt., vol.46, no.13, pp.2516–2519, 2007.

[15] S.M. Tripathi, A. Kumar, R.K. Varshney, Y.B.P. Kumar, E. Marin, and J.P. Meunier, "Strain and temperature sensing characteristics of single-mode-multimode-single-mode structures," J. Lightwave Technol., vol.27, no.13, pp.2348–2356, 2009.

[16] A. Kumar, R.K. Varshney, C.S. Antony, and P. Sharma, "Transmission characteristics of SMS fiber optic sensor structures," Opt. Commun., vol.219, no.1-6, pp.215–219, 2003.

[17] J. Huang, X. Lan, H. Wang, L. Yuan, T. Wei, Z. Gao, and H. Xiao, "Polymer optical fiber for large strain measurement based on multimode interference," Opt. Lett., vol.37, no.20, pp.4308–4310, 2012.

[18] Y. Koike and M. Asai, "The future of plastic optical fiber," NPG Asia Master., vol.1, no.1, pp.22–28, 2009.

[19] Y. Mizuno and K. Nakamura, "Experimental study of Brillouin scattering in perfluorinated polymer optical fiber at telecommunication wavelength," Appl. Phys. Lett., vol.97, no.2, 021103, 2010.

[20] Y. Mizuno and K. Nakamura, "Potential of Brillouin scattering in polymer optical fiber for strain-insensitive high-accuracy temperature sensing," Opt. Lett., vol.35, no.23, pp.3985–3987, 2010.

[21] Y. Mizuno, N. Hayashi, and K. Nakamura, "Brillouin scattering signal in polymer optical fiber enhanced by exploiting pulsed pump with multimode-fiber-assisted coupling technique," Opt. Lett., vol.38, no.9, pp.1467–1469, 2013.

[22] Y. Mizuno, N. Hayashi, H. Tanaka, K. Nakamura, and S. Todoroki, "Observation of polymer optical fiber fuse," Appl. Phys. Lett., vol.104, no.4, 043302, 2014.

[23] Y. Mizuno, N. Hayashi, H. Fukuda, K.Y. Song, and K. Nakamura, "Ultrahigh-speed distributed Brillouin reflectometry," Light: Sci.

Appl., vol.5, no.12, e16184, 2016.
[24] G. Numata, N. Hayashi, M. Tabaru, Y. Mizuno, and K. Nakamura, "Ultra-sensitive strain and temperature sensing based on modal interference in perfluorinated polymer optical fibers," IEEE Photon. J., vol.6, no.5, 6802306, 2014.
[25] T. Kawa, G. Numata, H. Lee, N. Hayashi, Y. Mizuno, and K. Nakamura, "Single-end-access strain and temperature sensing based on multimodal interference in polymer optical fibers," IEICE Electron. Express, vol.14, no.3, 20161239, 2017.
[26] G. Numata, N. Hayashi, M. Tabaru, Y. Mizuno, and K. Nakamura, "Drastic sensitivity enhancement of temperature sensing based on multimodal interference in polymer optical fibers," Appl. Phys. Express, vol.8, no.7, 072502, 2015.
[27] M. Naritomi, H. Murofushi, and N. Nakashima, "Dopants for a perfluorinated graded index polymer optical fiber," Bull. Chem. Soc. Jpn., vol.77, no.11, pp.2121–2127, 2004.
[28] W. Zou, Z. He, and K. Hotate, "Complete discrimination of strain and temperature using Brillouin frequency shift and birefringence in a polarization-maintaining fiber," Opt. Express, vol.17, no.3, pp.1248–1255, 2009.
[29] K. Minakawa, N. Hayashi, Y. Shinohara, M. Tahara, H. Hosoda, Y. Mizuno, and K. Nakamura, "Wide-range temperature dependences of Brillouin scattering properties in polymer optical fiber," Jpn. J. Appl. Phys., vol.53, no.4, 042502, 2014.
[30] K. Koike, H. Teng, Y. Koike, and Y. Okamoto, "Effect of dopant structure on refractive index and glass transition temperature of polymeric fiber-optic materials," Polym. Adv. Technol., vol.25, no.2, pp.204–210, 2014.
[31] E. Li, X. Wang, and C. Zhang, "Fiber-optic temperature sensor based on interference of selective higher-order modes," Appl. Phys. Lett., vol.89, no.9, 091119, 2006.
[32] R.M. Ribeiro and M.M. Werneck, "An intrinsic graded-index multimode optical fibre strain-gauge," Sens. Actuators A, vol.111, no.2-3, pp.210–215, 2004.
[33] T. Kawa, G. Numata, H. Lee, N. Hayashi, Y. Mizuno, and K. Nakamura, "Temperature sensing based on multimodal interference in polymer optical fibers: Room-temperature sensitivity enhancement by annealing," Jpn. J. Appl. Phys., vol.56, no.7, 078002, 2017.
[34] G. Numata, N. Hayashi, M. Tabaru, Y. Mizuno, and K. Nakamura, "Strain and temperature sensing based on multimode interference in partially chlorinated polymer optical fibers," IEICE Electron. Express, vol.12, no.2, 20141173, 2015.
[35] N. Hayashi, K. Minakawa, Y. Mizuno, and K. Nakamura, "Brillouin frequency shift hopping in polymer optical fiber," Appl. Phys. Lett., vol.105, no.9, 091113, 2014.
[36] K. Minakawa, Y. Mizuno, and K. Nakamura, "Cross effect of strain and temperature on Brillouin frequency shift in polymer optical fibers," J. Lightwave Technol., vol.35, no.12, pp.2481–2486, 2017.

Yosuke Mizuno received B.E., M.E., and Dr.Eng. degrees in electronic engineering from the University of Tokyo, Japan, in 2005, 2007, and 2010, respectively. From 2010 to 2012, as a Research Fellow (PD) of the Japan Society for the Promotion of Science (JSPS), he worked on polymer optics at Tokyo Institute of Technology, Japan. In 2011, he stayed at BAM Federal Institute for Materials Research and Testing, Germany, as a Visiting Research Associate. Since 2012, he has been an Assistant Professor at the Precision and Intelligence Laboratory (presently, Institute of Innovative Research), Tokyo Institute of Technology, where he is active in fiber-optic sensing, polymer optics, and ultrasonics. He is a senior member of the IEEE Photonics Society, and a member of the Japan Society of Applied Physics (JSAP), the Optical Society of Japan (OSJ), and the Institute of Electronics, Information, and Communication Engineers (IEICE) of Japan.

Goki Numata received a B.E. degree from Shibaura Institute of Technology, Tokyo, Japan, in 2014, and an M.E. degree from Tokyo Institute of Technology, Tokyo, Japan, in 2016. He is the winner of the Outstanding Student Award 2014, Opto-Electronics Conference (OPE), the Institute of Electronics, Information, and Communication Engineers (IEICE) of Japan. He is currently working at Olympus Corporation as an electronics engineer.

Tomohito Kawa received a B.E. degree from Tokyo Institute of Technology, Tokyo, Japan, in 2016. He is currently studying polymer fiber optics for his M.E. degree at Tokyo Institute of Technology. His research interests include fiber-optic sensors and polymer optics. He is a member of the Japan Society of Applied Physics (JSAP).

Heeyoung Lee received a B.E. degree in mechanical engineering from Kyungpook National University, Korea, in 2014, and an M.E. degree in information processing from Tokyo Institute of Technology, Japan, in 2017. Since 2017, she has been continuing to study fiber-optic sensors for her Dr.Eng. degree at Tokyo Institute of Technology. She is a Research Fellow (DC1) of the Japan Society for the Promotion of Science (JSPS) and a member of the Japan Society of Applied Physics (JSAP).

Neisei Hayashi received a B.E. degree in advanced production from the Gunma National College of Technology, Japan, in 2011, and M.E. and Dr.Eng degrees in electronic engineering from Tokyo Institute of Technology, Japan, in 2013 and 2015, respectively. Since 2016, as a Research Fellow (PD) of the Japan Society for the Promotion of Science (JSPS), he has been continuing to study fiber sensing at the University of Tokyo, Japan. His research interests include fiber-optic sensing, polymer optics, and nonlinear optics. He is the winner of the Telecom System Technology Award for Student 2012 and the NF Foundation R&D Encouragement Award 2016. He is a member of the Japan Society of Applied Physics (JSAP), and the Institute of Electronics, Information, and Communication Engineers (IEICE) of Japan.

Kentaro Nakamura received B.E., M.E., and Dr.Eng. degrees from Tokyo Institute of Technology, Japan, in 1987, 1989, and 1992, respectively. Since 2010, he has been a Professor at the Precision and Intelligence Laboratory (presently, Institute of Innovative Research), Tokyo Institute of Technology. His research field is the applications of ultrasonic waves, measurement of vibration and sound using optical methods, and fiber-optic sensing. He is the winner of the Awaya Kiyoshi Award for Encouragement of Research from the Acoustical Society of Japan (ASJ) in 1996, and the Best Paper Awards from the Institute of Electronics, Information and Communication Engineers (IEICE) in 1998 and from the Symposium on Ultrasonic Electronics (USE) in 2007 and 2011. He is a member of the IEEE, the ASJ, the Japan Society of Applied Physics (JSAP), the IEICE, and the Institute of Electrical Engineers of Japan (IEEJ).